# Impact of Sampling Method and Scale on the Measurement of Mixing and the Coefficient of Variance

**Alena Kukuková, Benjamin Noël, and Suzanne M. Kresta**
Dept. of Chemical and Materials Engineering, University of Alberta, Edmonton, Alberta, Canada, T6G 2G6

**Joelle Aubin**
Laboratoire de Génie Chimique CNRS/INPT/UPS, Université de Toulouse, 6 allée Emile Monso BP-34038, 31029 Toulouse Cedex 4, France

*DOI 10.1002/aic.11639*
*Published online October 29, 2008 in Wiley InterScience (www.interscience.wiley.com).*

*Spatial statistics methods are used to determine the effect of the sampling scale and method on two measures of mixing: the coefficient of variance CoV and the maximum striation thickness. Three sampling methods: quadrats, probes and transects, were tested. Two CFD data sets were used as test cases: dispersion of floating particles in a turbulent stirred tank and laminar mixing of tracer particles in a micromixer. Over 100 probes are needed to track the evolution of the CoV, and the probe size should match the smallest mixing scale of interest. The final value of the CoV varies by up to a factor of 5 as the probe size increases. The most useful measurement is the one which changes the most in the later stages of mixing: intensity of segregation, or CoV, for the turbulent case; and scale of segregation, or maximum striation thickness on a transect, for the laminar case.* © 2008 American Institute of Chemical Engineers *AIChE J,* 54: 3068–3083, 2008

*Keywords: mixing, blend time, intensity of segregation, scale of segregation, stirred tank, micromixer, static mixer, coefficient of variance, spatial statistics, striation thickness*

## Introduction

Many measures of the impact of mixing have been proposed in the literature, including mixing entropy,[1] various dimensions of chaotic flows,[2,3] Bourne micromixing and reaction models,[4] and population balance models[5,6] of drop breakup. In this article, it is not our intent to review all of these methods in detail, but rather to focus on the accurate determination of two measures of mixing: the *CoV*, which is used directly for the design of static mixers, and indirectly for determination of the blend time in stirred tanks, and the maximum striation thickness on a transect, which is of significant interest as a contrasting measure, particularly for laminar mixing.[7]

Danckwerts[8] defined two extreme states of mixedness: complete and instantaneous mixing on the molecular scale, and complete segregation. Danckwerts gives a description of complete segregation, "The incoming fluid is broken up into discrete fragments or streaks which are small compared to the tank and uniformly dispersed in it, but in which molecules entering together remain together indefinitely." This might be physically realized as drops of one component A, and a second component B, both suspended in an inert medium in which they are both completely insoluble, and where no coalescence can occur. In the completely segregated case, the size of the drops does not matter, but in many real flows and practical applications the size of the segregated regions is critically important, and molecules are neither completely

Correspondence concerning this article should be addressed to S. Kresta at Suzanne.kresta@ualberta.ca.

segregated nor perfectly mixed. Moreover, real times greater than zero and smaller than infinity are of interest.

Danckwerts' initial ideas eventually evolved into the definition of various mixing scales which are now widely used in the mixing literature. Macromixing is identified with the scale of the equipment, e.g., the tank diameter, and with the blend time. Mesomixing occurs at intermediate scales and is identified primarily with reaction effects due to mixing limitations in the feed plume. Micromixing is identified with the smallest scales of motion and concentration segregation, where molecular viscosity and diffusivity dominate. These definitions have proven difficult to explain to nonexperts, which suggests that their current formulation is somewhat less than crystal clear. This difficulty is partly due to the differences between mixing in turbulent flows and mixing in laminar flows. In this article, the two regimes are compared side-by-side to highlight the differences and similarities in their behavior.

Turbulent mixing is a complex multiscale process ranging from macromixing on the scale of the vessel, usually characterized as the blend time, to micromixing on the scale of the smallest eddies, often characterized using the Kolmogorov time scale, or the engulfment rate.[4] Turbulence is three-dimensional (3-D), random, and time varying, and is normally characterized using the local mean and rms (standard deviation) of the velocity and concentration. A statistical approach, is, therefore, a natural fit to the characterization of turbulent mixing, and point-based statistics collected over time have been applied to turbulent mixing for many decades.

Laminar mixing is ultimately limited by molecular diffusion. For efficient mixing, the fluids must be manipulated to increase the interfacial area, and decrease the thickness of fluid lamellae in order to promote diffusional mixing. Laminar mixing measurements need to be able to resolve the fine structures of the fluid lamellae. Some spatial statistics and similarity analyses have been applied to this problem, but characterization methods that are both practical and powerful are still a subject of active research.[9]

The field of spatial statistics[10] includes applications ranging from population ecology to the study of human populations, disease, and racial segregation, to forestry and geostatistics. All of these applications have one thing in common: the underlying data has a complex pattern, and the local concentration of each species is of interest for understanding the problem. Spatial statistics provides a set of knowledge not previously applied to mixing problems in the field of chemical engineering. Two principles are of particular interest. First, mixing is a multidimensional problem which cannot be completely characterized with a single variable, or dimension. Second, the goal of statistical analysis is to extract the maximum information from the minimum amount of data. The penalty to be paid for this efficient use of data is that the sampling method becomes very important.

From a review of the wide ranging literature on spatial statistics, three dimensions of segregation emerge as important to the study of mixing in chemical processes: the scale of segregation, the intensity of segregation, and the exposure.[11] The scale of segregation is most easily defined for this article as the striation thickness distribution. The intensity of segregation is directly related to the *CoV*. The exposure dimension is related to the ease and rate of reduction in segregation but is not of interest for this article. A simple thought experiment is used to illustrate the importance of distinguishing between the intensity and scale of segregation. Taking a square that measures 16 mm × 16 mm, consider two mixing fields: in the first, there are four squares which measure 8 mm × 8 mm each, two of them black and two of them white; in the second, there are 256 squares each measuring 1 mm × 1 mm, again, half black and half white. Both fields are arranged in a checkerboard pattern. We might quickly conclude that the mixing is better in the second case because the scale of segregation has been reduced by a factor of 8, but calculation of the *CoV* will return exactly the same result for both mixing fields. The intensity of segregation is independent of how the squares are arranged. Further exploration of this example shows that the scale of averaging used to calculate the *CoV* can also dramatically affect the result.[11]

In this work, two test cases were used to evaluate two measures of "well-mixed": the *CoV*, which characterizes the intensity of segregation, and the maximum striation thickness, which characterizes the scale of segregation. The objectives of the investigation are:

1. to explore the data density and sampling protocols needed to get accurate measures of *CoV* for two ideal data sets,
2. to explore the data density needed to get an accurate measure of striation thickness for the same data sets,
3. to compare the *CoV* and the maximum striation thickness for laminar mixing at a very small scale, and turbulent mixing at a relatively large scale to better understand the strengths and weaknesses of each approach.

Before detailing the test cases and the sampling experiments which were performed, the definitions and background theory for the coefficient of variance and for the three sampling strategies of interest are reviewed.

### *Definition of the coefficient of variance*

Two quantities are widely used in the mixing literature to evaluate the intensity of segregation: the blend time for batch-stirred tanks and the decay of the coefficient of variance ($CoV_r$) in continuous static mixers. Both measures are evaluated from concentration measurements at several locations.

The batch-blend time is based on the decay of the *normalized* concentration variance

$$\sigma_M^2(t) = \frac{1}{M}\sum_{m=1}^{M}\left(\frac{C_m - C_{m,0}}{\overline{C} - C_{m,0}} - 1\right)^2 \tag{1}$$

where $C_{m,0}$ is the initial concentration at probe $m$, $C_m$ is the concentration at time $t$, $\overline{C}$ is the average concentration for a homogeneous mixture, and $M$ is the number of measurement locations. When the initial concentration is zero at all measurement locations, Eq. 1 reduces to

$$\log(\sigma_M^2) = \log\left[\frac{\sum_{m=1}^{M}(C_m - \overline{C})^2}{M\overline{C}^2}\right] \tag{2}$$

The blend time is defined as the time when $\sigma_M^2 = 0.0025$ and $\sigma_M^2 = -2.6$, which is a 95% approach to the perfectly mixed state.[12]

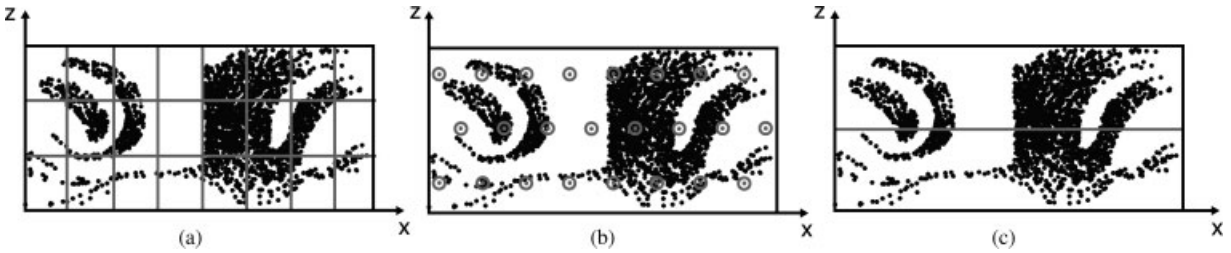


**Figure 1. Illustration of sampling strategies: (a) rectangular quadrats, (b) point probes, and (c) transect of width $\Delta z$.**

The second measure of intensity of segregation is known as the *CoV*, or the coefficient of variance. This criterion is usually applied to static mixers, particularly for laminar blending applications. The *CoV* is the ratio of the standard deviation of the concentration measurements to the mean concentration,[13] and it is exactly equal to the square root of the blend time variance decay criterion

$$CoV = \frac{\sigma}{\overline{C}} \frac{\sqrt{\frac{1}{M}\sum_{m=1}^{M}(C_m - \overline{C})^2}}{\overline{C}} = \sigma_M \tag{3}$$

In this case, a well mixed threshold corresponding to 95% of the perfectly mixed state can also be set such that $\sigma_M^2 = 0.0025$.

Laminar static mixer data for a well designed mixer typically follows an exponential decay of the *CoV* following the relations[14]

$$CoV_0 = \left(\frac{1 - C_v}{C_v}\right)^{0.5} \tag{4}$$

$$CoV = CoV_0 K^{L/D} \tag{5}$$

$$CoV_r = \frac{CoV}{CoV_0} = K^{L/D} \tag{6}$$

where $C_v$ is the volume fraction of unmixed additive. $CoV_0$ is 1.0 for 50% additive and increases to 3 for 10% additive. Using $CoV_r$ collapses the data for static mixers onto a single line for a range of inlet concentrations.

Both definitions of *CoV* require the use of multiple concentration samples, but minimal guidance is available as to the required number of samples, or regarding limitations on the size of the probe. To resolve some of these questions, we begin by reviewing what is known about sampling requirements for spatial statistics.

### *Sampling methods used for spatial statistics*

In order to calculate the intensity of segregation, a concentration data set must be extracted from a three-dimensional (3-D) mixing field. Two types of concentration data are available from experiments and/or numerical simulations. The first is the concentration of a second chemical species, the second is the concentration of tracer particles which have been released into the mixing field. Where a full 3-D data set is not available, a representative plane must be selected, and where a full plane of data is not available, a representative transect or traverse or a set of sampling points may be selected. As the available data becomes sparser, the sampling method and statistical analysis become more important. The choice of the sampling strategy will be constrained by the amount of data available, but it must also be well matched to the problem statement and definition.

Figure 1 illustrates three classes of sampling strategies used in spatial statistics: quadrats, probes and transects. The term quadrat was originally defined as a 1 m $\times$ 1 m sample area for ecological studies.[15] Today, the term quadrat refers to any 2-D sample area. Its size and shape is arbitrary, and is not necessarily uniform (e.g., census data). Quadrat sampling covers a full plane of data: in statistical terms it is an *area filling* sampling method. Point probes are mathematically zero dimensional, in the sense that they are centered at a point in space and occupy no volume. Practically, however, they must have a finite sampling area or measurement volume in order to sample a physically and statistically meaningful number of molecules, or tracer particles.[8] Transects are 1-D and traverse the measurement volume along a single line. Again, the line is mathematically of zero thickness, but a finite width is required to sample a statistically and physically meaningful number of real particles or molecules. The purpose of the transect sample differs from the quadrat and probe samples. Although the mean and variance along the transect can be calculated to give a measure of the intensity of segregation, the transect is primarily used to profile concentration,[16] and to determine a striation thickness distribution, thus, giving information about the scales of segregation. Quadrats, probes, and transects can all be used to sample either a plane or a volume of data.

In quadrat analysis, the plane of interest is divided into a number of areas (quadrats), often of the same size and shape. The number of quadrats, and, thus, their size, depends on the desired level of spatial resolution. Ideally, the concentration in a quadrat is uniform and the quadrat size is matched to the smallest scale of the concentration striations. However, this is not always possible, either because the smallest scales are unknown, or because it is not possible to measure concentration with such a high-resolution. When the quadrat is larger than the local scale of segregation, the mean quadrat concentration depends on the size and shape of the quadrat. This dilemma, most simply illustrated by the checkerboard thought experiment, causes a number of difficulties for analysis, and is known as the modifiable areal unit problem (MAUP) in population studies. It is discussed in some detail in the literature.[17–20] Once the size and shape of the quadrats has been defined, the mean concentration in each quadrat is

calculated from the raw data. The *CoV* is then evaluated using Eq. 3, where $M$ is now the number of quadrats.

When using probes to get concentration data, a set of probe locations is selected. As with the quadrat selection, some attention to the sampling strategy is warranted. If the underlying data has a regular pattern, the probe locations must either be randomized, or there must be enough probes to accurately sample the entire mixing field. When the data set is complete and the mixing field is either irregular or can be densely sampled, a regular sampling grid is both useful and efficient. If the number of probes available is very limited, however; as is the case for typical blend time measurements, then the probe placement must be based on sound physical reasoning and an understanding of the process. At least one of the probes must be located in the last-mixed region if accurate blend times are to be obtained.[12]

Once the probe locations are selected, the probe size must be identified. Ideally, the probe size should match the smallest scales of mixing that are to be measured, however; practical limitations mean that the scale of resolution of the measurement method is usually limited by the actual size of the probe. If a physical probe is used, the concentration is averaged over the measurement volume and is assumed to be uniform within the measurement volume. If a CFD simulation is used with scalar transport, the concentration is averaged over the cell volume. If CFD with particle tracking is used, the resolution of particle motion is limited by the step size in the particle paths, and the resolution of striations at any instant in time is limited by the number of particles in the simulation. When particle concentration is calculated from discrete particle data, the particle concentration is based on the number of particles in the probe. The probe size should be small enough to get local data, but also large enough to contain a statistically significant number of particles. As a result, the smallest scale of resolution of the concentration probes is limited by the number of particles in the simulation. To avoid counting tracking particles twice, the probe areas should not overlap, so the maximum probe size is limited by the number of points in the sampling grid.

To get the most valuable information about mixing, a transect should pass through the worst mixed part of the mixing field, and as much as possible should be oriented to be perpendicular to the striations of greatest interest. A transect has two variable dimensions: the width of the transect $\Delta z$, and the striation thickness threshold. In forestry studies, the width of a foresters' arms, or a $\Delta z = 2$ m is used to sample a forest. A particle is included in the transect if its $z$-coordinate equals the $z$-coordinate of the transect $\pm\ \Delta z/2$. Aubin et al.[7] selected a transect width, $\Delta z$, equal to the mean particle spacing in the mixing field. The width of the transect, $\Delta z$, allows for the capture of a single particle, and transect sampling then assumes that all particles in the 2-D transect are associated with the equivalent 1-D line through the mixing field.

The striation thicknesses on the transect are determined using the function $f$, which has the following properties

$$\begin{aligned} \Delta x(\text{neighbours}) \leq \Delta x: &\quad f(x) = 1 \\ \Delta x(\text{neighbours}) > \Delta x: &\quad f(x) = 0 \end{aligned} \tag{7}$$

Striation thicknesses on the transect are calculated directly from the function $f(x)$: when two consecutive particles in the transect are within $\Delta x$ of each other, they are both in the same striation. If $\Delta x$ is too large, the striations will be unrealistically large; if it is too small, no striations will be detected. In a real striation, the particles will be closer together than the mean particle spacing, so we expect the $\Delta x$ value to be smaller than the $\Delta z$ value. If concentration data are used to determine striation thickness distributions on a transect, a concentration threshold must be defined to replace $\Delta x$, the threshold distance between tracking particles. No full-field concentration data is available to test this thresholding requirement in the current work, but some initial thresholding work in the time domain is reported by Hilderman and Wilson[21] and Hilderman et al.[22] Note that the statistical and mathematical analyses of transects through time at a single point in space, and transects through space at a single instant in time are the same.[10]

## Experimental

The *CoV* obtained from both probe and quadrat sampling methods, and the maximum striation thickness measured on a transect are all affected by the size and shape of the sample. Probe sampling can be affected by the location, number, and size of the probes, while quadrat sampling requires attention to the modifiable areal unit problem, MAUP. Transects require the user to define the threshold value for particle separation, and the width of the transect. These requirements are well documented in other fields of study, as discussed earlier in the article.

The two objectives of the sampling experiment are to compare quadrat and probe sampling methods in the context of blend time calculations for two test cases, and to compare measurements of the scale and intensity of segregation. Quadrat and probe sampling are compared on the basis of number of probes or quadrats, size of probes or quadrats, and the resulting *CoV*. Transect sampling is explored for different transect widths and separation thresholds to determine the effect of spatial resolution on the maximum striation thickness. The results are compared globally to better understand what each measure reveals about mixing.

### *Test cases*

Two test cases were used to study the effect of sampling on measurements of mixing. The first test case is the dispersion and dissolution of floating particles in a turbulent stirred tank, shown in Figure 2 and Figure 3. The second test case is the laminar mixing of massless tracer particles in a staggered herringbone micromixer, shown in Figure 4. These test cases represent two extremes of scale (tank dia. $T = 0.2335$ m, and the micromixer width $w = 200$ $\mu$m); two extremes of mixing and dispersion (multiphase turbulent mixing and dissolution in the first case; single-phase laminar blending in the second); and widely varying data densities ($7 \times 10^6$ particles vs. 2,480 particles). In both cases, planes of data are extracted from three-dimensional CFD simulations of mixing. These simulations provide exceptionally complete data sets for the evaluation of statistical sampling and data analysis methods.

The first test case is the dispersion and dissolution of floating particles suspended in a tank stirred by a Rushton

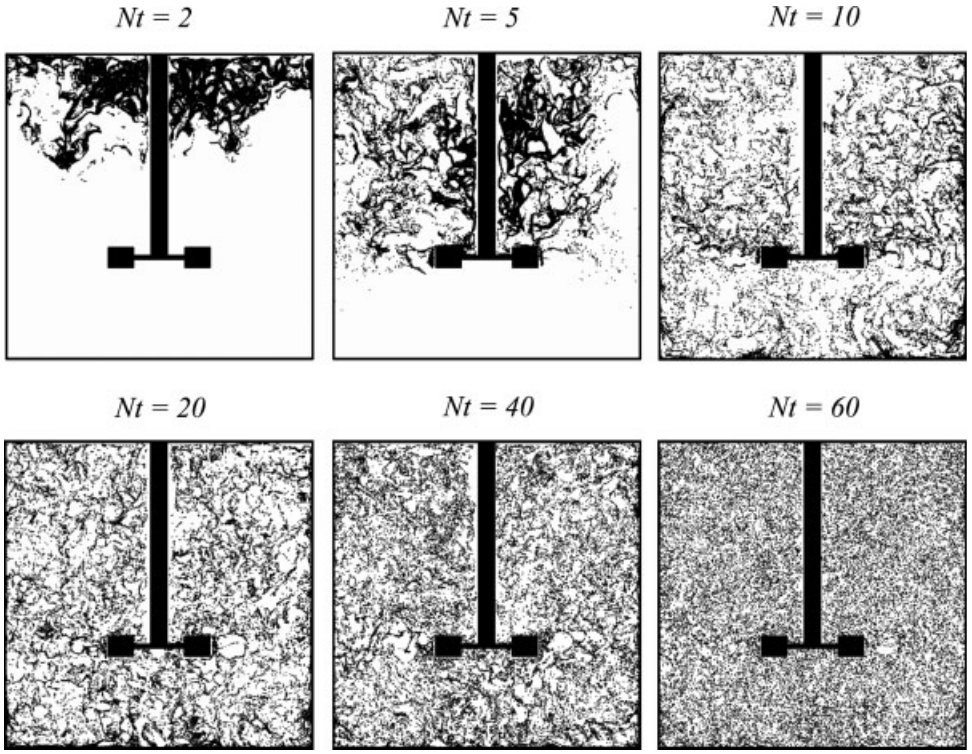


**Figure 2. Particle distribution in the mid-baffle plane of the turbulent stirred tank, $T$ = 0.2335 m, $D = T/3$, $C = T/3$, $N$ = 990 rpm; $Nt$ = number of impeller revolutions.**

turbine. The cylindrical, flat bottomed tank has a dia. $T$ = 0.2335, and is fitted with four standard baffles of width $0.1T$, and a six-bladed Rushton turbine impeller of dia. $D = T/3$. The impeller is mounted at height of $C_{imp} = T/3$ above the vessel bottom, and rotates at a speed of $N$ = 990 rpm (fully turbulent). It was filled with water ($\rho_l$ = 1,000 kg/m$^3$) to a height of $H = T$. At the beginning of the simulation, 7 × $10^6$ monodisperse spherical particles with dia. $d_p$ = 0.3 mm

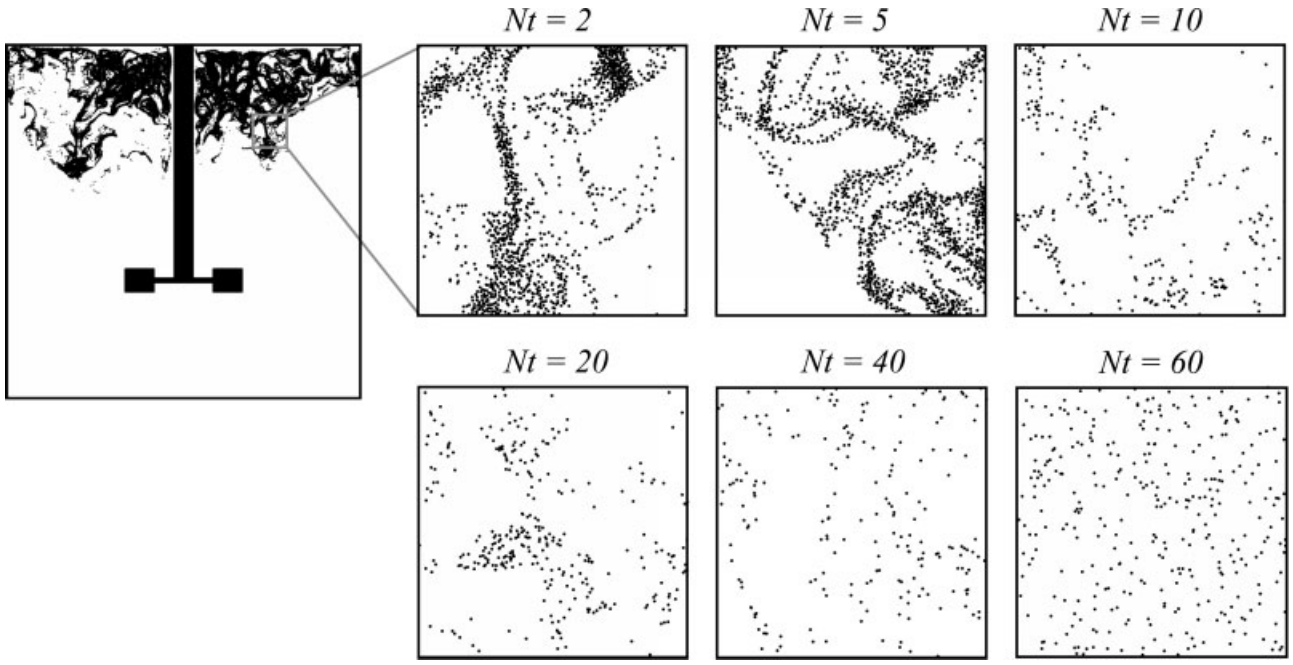


**Figure 3. Magnified view of the particle distribution in a window $T/10 \times T/10$ big centered at $r = T/4$, and $z$ (axial coordinate) = $0.75T$.**

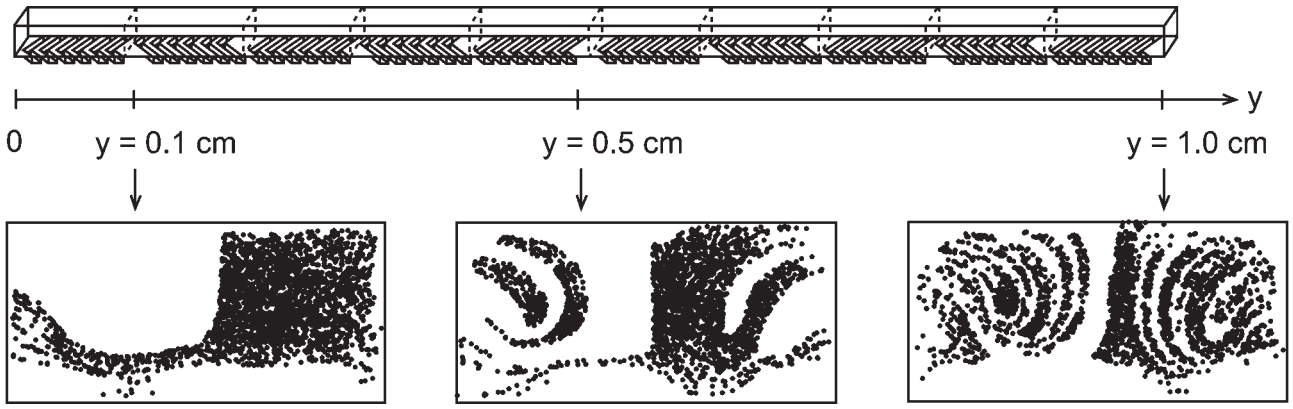


**Figure 4. Geometry of the rectangular micromixer.**

Channel height ($h$ = 77 $\mu$m), and channel width ($w$ = 200 $\mu$m). Three groove depths are tested ($d_g$ = 0.23$h$, 0.30$h$, and 0.35$h$). The three cross sectional sampling planes at three locations along the laminar micromixer illustrate the particle distribution for a groove depth of 0.23$h$.

and density $\rho_p$ = 2,150 kg/m$^3$ were released in the upper part of the tank. The particle distribution and dissolution simulation was performed using a transient large eddy simulation with the Eulerian-Lagrangian particle tracking approach. More details about the simulation can be found in the article by Hartmann et al.[23] Figure 2 and Figure 3 show the data set extracted from the simulation for analysis: particle positions in a vertical cross-section mid-way between two baffles at six different times during the simulation. In this case, the particles dissolve and move randomly in and out of the sampling plane, and as a result the number of particles in the slice varies between 28,000 and 56,000. Figure 3 illustrates the spatial resolution of the simulation: in this case a mean particle separation of 1 mm, or roughly 0.5% of the tank diameter.

The second test case is laminar mixing in a staggered herringbone micromixer, as shown in Figure 4. The mixer is a rectangular channel with a width of $w$ = 200 $\mu$m, height $h$ = 77 $\mu$m, and length $L$ = 0.01 m, with grooves of depth $d_g$ = 0.23$h$, 0.30$h$ and 0.35$h$, and width $W_g$ = 50 $\mu$m. A total of 2,480 uniformly distributed massless particles were placed on the righthand side of the solved flow field at the mixer inlet, and were followed using the Lagrangian particle tracking method. A restitution coefficient of unity is applied to the microchannel walls. This avoids particle trajectories being trapped near the walls where the local velocity is close to zero (less than 2% of particles are stopped between the inlet and the outlet of the mixer). The details of the simulation procedure are described by Aubin et al.[7] The objective of the simulation is to compare the mixing efficiency for three different groove depths. Vertical planes along the micromixer were sampled at intervals of 100 $\mu$m in order to compare the designs.

### *Sampling experiments*

The first sampling method considered is probes. Figure 5 shows the regular hexagonal grid[7] used to set the probe locations in both the tank and the micromixer. For the stirred tank case, grids containing 36, 142, 274, 536, 1,093 and 2,209 probe points were tested. The points located in the shaft and impeller areas were omitted. The probe area $A_k$ was set equal to the area of a circle that would contain a fixed number of particles, $k$, in a perfectly homogeneous distribution

$$A_k = k\frac{A}{p} \tag{8}$$

where $A$ is the area of the slice minus the area of the impeller and shaft, and $p$ is the total number of particles in the slice. Three aspects of the probe sampling were studied here; namely the effect of the probe location, size, and number. To investigate the effect of probe location, six sets of three probes were selected as shown in Figure 6. The probe locations are summarized in Table 1. To analyze the effect of the probe size on the resulting $CoV$, the 536-probe grid was used with probe sizes of $k$ = 3, 10, 30 and 180 particles. The effect of the number of probes was studied by calculating the $CoV$ for all grids with a constant 10-particle-probe size ($k$ = 10). For the micromixer case, only the effects of probe number (using hexagonal grids of 30, 60, 105, 198 and 640 points), and probe size ($k$ = 3, 5, 10, 20, 50) on the $CoV$ were evaluated.

The effects of the quadrat sampling parameters on $CoV$ were studied using the herringbone micromixer test case. At each cross-sectional plane along the micromixer, the data

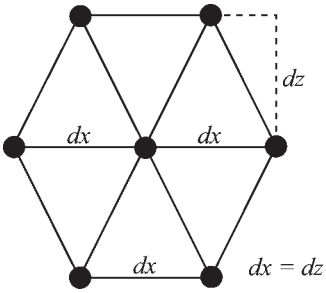


**Figure 5. Hexagonal grid used for setting probe locations in the stirred tank and the micromixer.**

In the tank $dx = dz$ and in the laminar micromixer $dx \approx dz$.

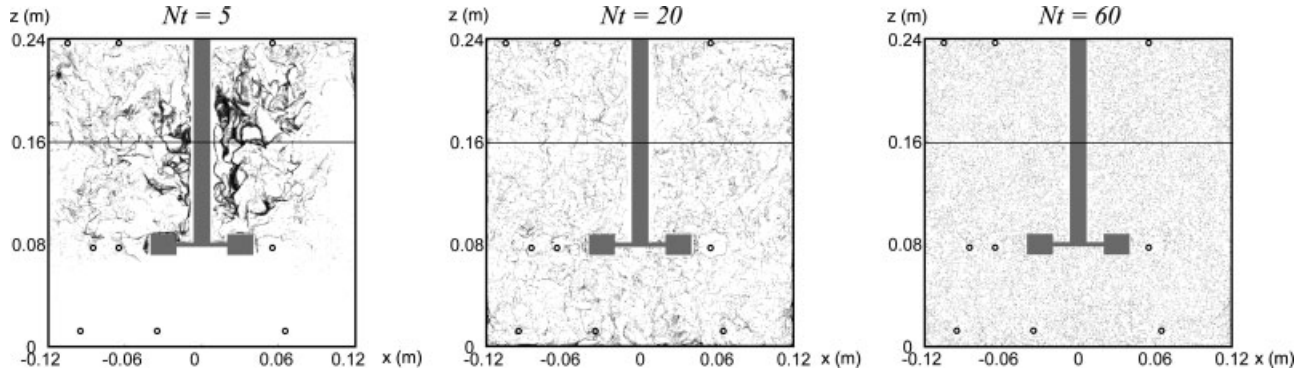


**Figure 6. Location and size of probes and transects at three time steps (*Nt* = 5, *d* = 3.59 mm; *Nt* = 20, *d* = 4.55 mm; *Nt* = 60, *d* = 4.89 mm, where *d* is the probe diameter).**

The transect is located at $z = 2T/3$. The nine probe positions are given in Table 1. Six sets of three probes are analyzed: the top three, center three, and bottom three; the left three, middle three, and right three.

was divided into 10, 24, 40 and 640 equal rectangular quadrats, and the *CoV* was calculated. Here, the quadrat size is inversely proportional to the number of quadrats (since quadrats cover the whole region of study). To compare the probe and quadrat analyses, the *CoV* was calculated from the grid containing 640 circular probes (with a maximum probe size of 2.92 particles per probe) and compared with the *CoV* calculated from 640 rectangular quadrats.

Transect sampling was used to determine the maximum striation thickness in both the stirred tank and the micromixer test cases. The maximum striation thickness on a transect in the stirred tank was calculated using Eq. 7. The transect was located at two thirds of the tank height, as shown in Figure 6. For the base case, the resolution in the axial direction, $\Delta z$, was set equal to the mean particle spacing for a perfectly homogeneous distribution of 39,330 particles

$$\Delta z = \sqrt{\frac{A}{p}} \cong 1 \text{ mm} \tag{9}$$

where $A$ is the area of the tank cross section after substracting the impeller and shaft areas and $p$ is the average number of particles in the data plane. The effect of transect width, $\Delta z$, on the maximum striation thickness was examined by varying $\Delta z = \Delta x = 0.5$ mm, 1 mm and 2 mm.

Different resolutions in the $x$-direction, $\Delta x$, were used to isolate the effect of $\Delta x$ on the striation thickness. The transect width was fixed at $\Delta z = 1$ mm for $\Delta x$ resolutions of 2 mm, 1 mm, 0.75 mm and 0.5 mm. A finer resolution would require more tracer particles, with the number of particles required increasing as $1/\Delta x^2$. For the staggered herringbone micromixer, the striation thickness calculation was performed using a single resolution of $\Delta z = \Delta y = 5$ $\mu$m, which is equal to the mean particle spacing given in Eq. 9.

## Results and Discussion

The case of the turbulent stirred tank with dissolving solid particles is discussed first, followed by the herringbone micromixer case. The effect of probe location on the *CoV* is illustrated first, using the stirred tank. Both cases are then used to explore the effect of probe number and size on the *CoV*. The maximum striation thickness on a transect is also calculated as the mixing evolves, using varying transect resolutions. In the laminar mixing case, probe and quadrat sampling strategies are compared and contrasted with the evolution of the maximum striation thickness on a transect. The results shed additional light on the information contained in the two different measures of mixing.

### *Turbulent mixing: CoV results*

There are no fixed criteria for selecting the number and location of probes for *CoV* measurements, and, thus, for the measurement of blend time, or the decay of intensity of segregation. In order to obtain full spatial resolution of the 3-D mixing field, a very large number of probes would be required. When a limited number of probes are available, at least one probe must be located in the worst-mixed part of the vessel if the *CoV* is to detect the final stages of mixing.[12] Figure 7 illustrates the impact of the probe location for the six different sets of three probes shown in Figure 6, and a seventh set of three randomly selected probe locations. These results are compared with the true *CoV* determined using 4,292 probes evenly spaced throughout the mixing field. For each set of three probes, the evolution of the *CoV* is different, and none of the sets of three probes tracks the true *CoV*. When three probes are used, as recommended in the blend

**Table 1. Positions of Probes used to Study the effect of Probe Location**

| $x$/m | $z$/m | used in sets |
|---|---|---|
| −0.1050 | 0.2375 | up, left |
| −0.0650 | 0.2375 | up, middle |
| 0.0550 | 0.2375 | up, right |
| −0.0850 | 0.0775 | center, left |
| −0.0650 | 0.0775 | center, middle |
| 0.0550 | 0.0775 | center, right |
| −0.0950 | 0.0125 | down, left |
| −0.0350 | 0.0125 | down, middle |
| 0.0650 | 0.0125 | down, right |

All probes lie in the vertical mid-baffle plane, $\theta = 0°$.

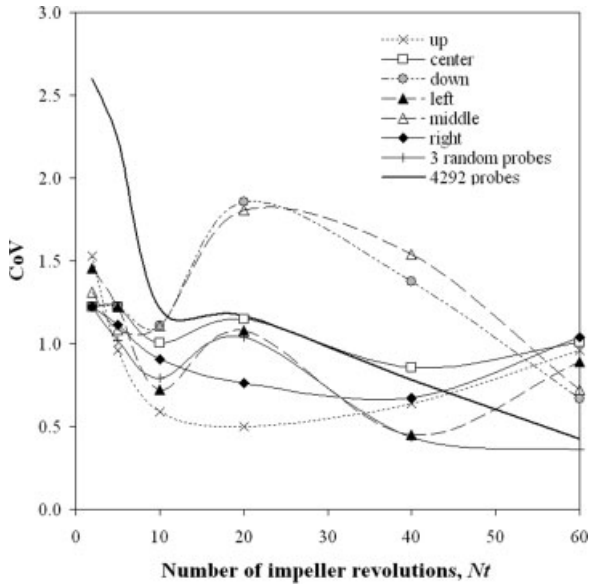


**Figure 7. *CoV* for the seven different sets of three 10-particle probes shown in Figure 6.**

The dark solid line for a large number of probes provides a reference to the true evolution of the *CoV* in the tank.

time protocol given by Brown et al[12] the evolution of the *CoV* strongly depends on the location of the probes.

Three probes are clearly not enough to correctly sample a complex mixing field. The next question to address is, "How many probes are needed, given an ideal data set?" As the number of probes increases, the *CoV* calculated from a full plane of data will approach the true *CoV* in the tank. In most experimental applications, the use of a large number of probes is impractical, and could change the flow field enough to endanger the accuracy of the measurement. The optimum balance between the number of probes and the accuracy of the *CoV* measurement is illustrated in Figure 8. For a small number of probes, the measured evolution of *CoV* is unreliable, but as the number of probes increases to 274 and beyond, the curves converge onto one curve which is representative of the whole population, as highlighted in Figure 8b.

Returning to Figure 8a, note that for $Nt \geq 40$, the curves for 36 probes or more converge. From this, one might conclude that for long times, or for a small threshold on the final *CoV*, even the curve for three probes may approach the true value. This is an important finding because if only a very small number of probes are available, then setting a "well mixed" criterion to a very small *CoV* value will ensure that the required degree of mixing is achieved. Referring back to the blend time protocol,[12] we find a very small equivalent *CoV* threshold of 0.0025. This conservative limit ensures that measured blend times are consistent between experimenters and provides an accurate measure of "complete mixedness" which scales up reliably. This is in agreement with both industrial experience, and a number of blend time articles in the open literature.[24–26]

While the data in this test case is for particle dispersion, rather than blend time, it is interesting to compare the blend time ($N\theta_{95} = 5.20/N_p^{1/3} \times (T/D)^2 = 27$ (Eq. 10)[24]) with these *CoV* curves. Note the rapid decay of *CoV* up to $Nt = 10$ — clearly the volume filling stage in Figure 2 — followed by the slower decay in *CoV* during the scale reduction phase. This suggests that the blend time, or the macromixing time, is primarily related to the inital dispersion of the tracer throughout the volume of the vessel, with a conservative design factor added in to compensate for the small number of probes. We might then redefine "macromixing" as the volume filling stage of mixing, "mesomixing" as the scale

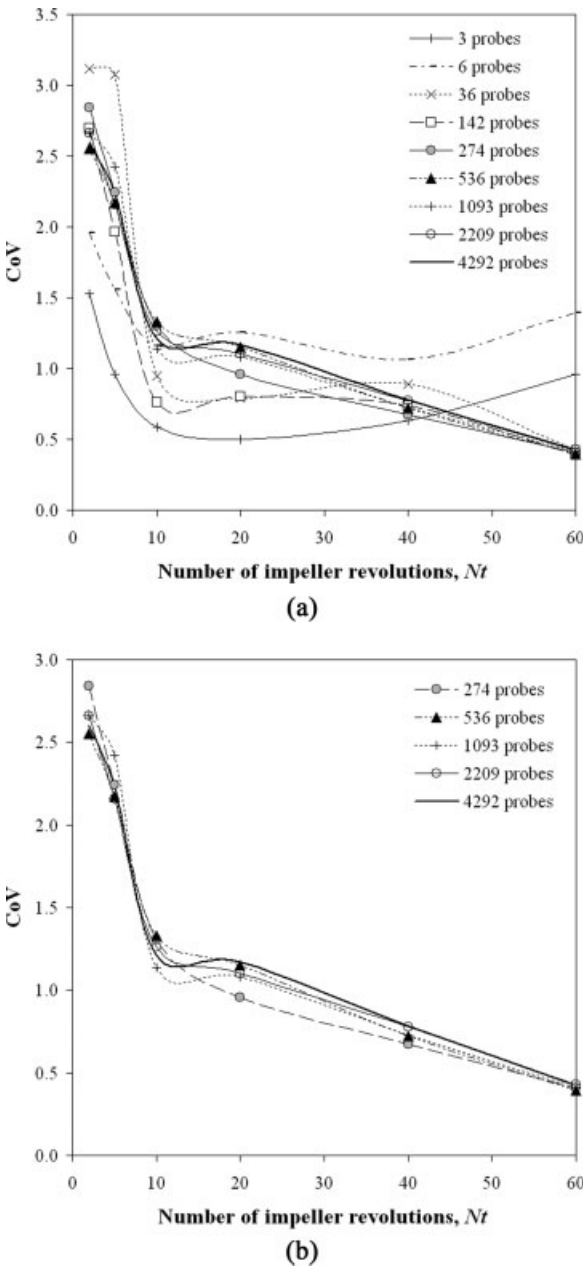


**Figure 8. Influence of the number of probes on *CoV*. A 10-particle probe size was used for each time step, causing the probe size to vary slightly as the number of particles in the plane varied over time.**

Figure 8a shows all of the data, while Figure 8b focuses on the data which is independent of the number of probes.

reduction stage, which in turbulent mixing is closely related to the inertial convective range of eddies, and "micromixing" as the stage of mixing when the scale of segregation is reduced to the point where molecular mechanisms, such as viscous dissipation and molecular diffusivity become dominant.

While the number of probes determines the total area sampled, the spatial resolution of the *CoV* measurement is determined by the probe size. In selecting the size of the probe for a fixed data set, two competing requirements must be satisfied. On the one hand, it is important to have enough particles in the probe to give a statistically meaningful result. If the probe contains only one or two particles on average, the data will be highly variable. On the other hand, if the probe is too big, it will contain many particles, but the spatial resolution of the measurement will be poor and many details of the mixing field will be lost. The goal should be to capture the required scales of mixing using the minimum number of tracking particles, whereas at the same time maintaining the statistical significance of the measurement.

Setting the mean number of particles in the probe volume to 10, under perfectly homogeneous conditions, means that a deviation from the mean of one particle will cause a 10% deviation in probe concentration. Using a 3-particle probe means that the probe size is smaller, and the concentration data has high-spatial resolution, but the importance of 1 particle is high, impacting the probe concentration by 33%. This will increase the measured variance significantly. One particle in a 100-particle probe only impacts the probe concentration by 1%, but at the expense of the low-spatial resolution of the probe.

Figure 9 shows the effect of the number of particles in the probe on the calculated *CoV*. As the number of particles increases, the probe size increases and the calculated *CoV* gets smaller. Spatial resolution is lost because the local concentration differences (striations or clusters) are averaged over the increasingly large probe volume. To get local data, the probe needs to be smaller than the smallest scale of interest, but large enough to contain a statistically meaningful number of particles. A 10-particle probe size was chosen for all subsequent calculations for the stirred-tank test case.

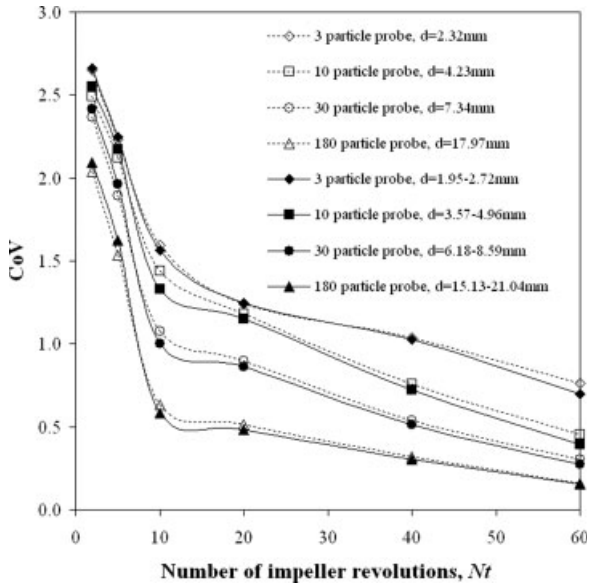


**Figure 9. Influence of the probe size on *CoV*.**

The open symbols correspond to a fixed probe diameter for all time steps, based on the average number of particles in the plane. The filled symbols correspond to a probe diameter which was allowed to vary with time, depending on the number of particles in the plane at that time step. The number of probes was ($M = 536$) for all calculations.

Because the particles in this simulation were tracked in three dimensions, and were allowed to dissolve over time, the number of particles in the data plane varied slightly. Two methods were used for setting the probe diameter. The first approach was to calculate the probe diameter from the average number of particles in the plane over all time steps. The result was a fixed probe diameter for all time steps for each *k*-particle probe. The second method used calculated the probe diameter at each time step for each *k*-particle probe. This results in a probe diameter that varies slightly over time. A comparison of the two approaches given in Figure 9 shows that there is no significant effect on the *CoV* curves.

In future studies, the probe size should first be set equal to the smallest scale of interest. The number of tracer particles required in the simulation can then be set to

$$p = \frac{4k}{\pi}\frac{A}{d^2} \tag{11}$$

which ensures that there will be *k*-particles in each probe when the mixing is perfectly homogeneous. This gives a clear physical meaning to the probe size, and ensures that the number of particles in the simulation is large enough to achieve the desired spatial resolution.

The *CoV* calculations for the stirred tank clearly show the limitations of using three probes for the measurement of *CoV*, particularly during the early stages of mixing when the mixing patterns are complex. The sensitivity of *CoV* to the diameter of the probe, or to the number of particles in the probe, emphasizes that *CoV* measures intensity of segregation, not scale of segregation; and that the probe size must be defined based on both the mixing field of interest and the spatial resolution required by the problem. To provide some direct insight into the scale of segregation, the measurement of striation thickness along a transect is considered next.

### *Turbulent mixing: Transect results*

Figure 10a–f present the function *f(x)* used to calculate the maximum striation thickness on a transect using different spatial resolutions in the *x*- and *z*-directions. All plots were created for the time step corresponding to 60 impeller revolutions, because at this time the particle distribution is the closest to a homogeneous distribution. The bar thicknesses correspond to the striation thicknesses along the transect. The plots also include a picture of the particle distribution in each transect. Note that the transect widths ($\Delta z$) are not to scale because in reality, they are so small that nothing would be visible from the correct scale.

The striation thicknesses determined with resolutions of $\Delta x = \Delta z = 2$ mm, shown in Figure 10a, indicate that there are very big striations inside the vessel, but visually, the distribution of particles at this time step is very good, as shown

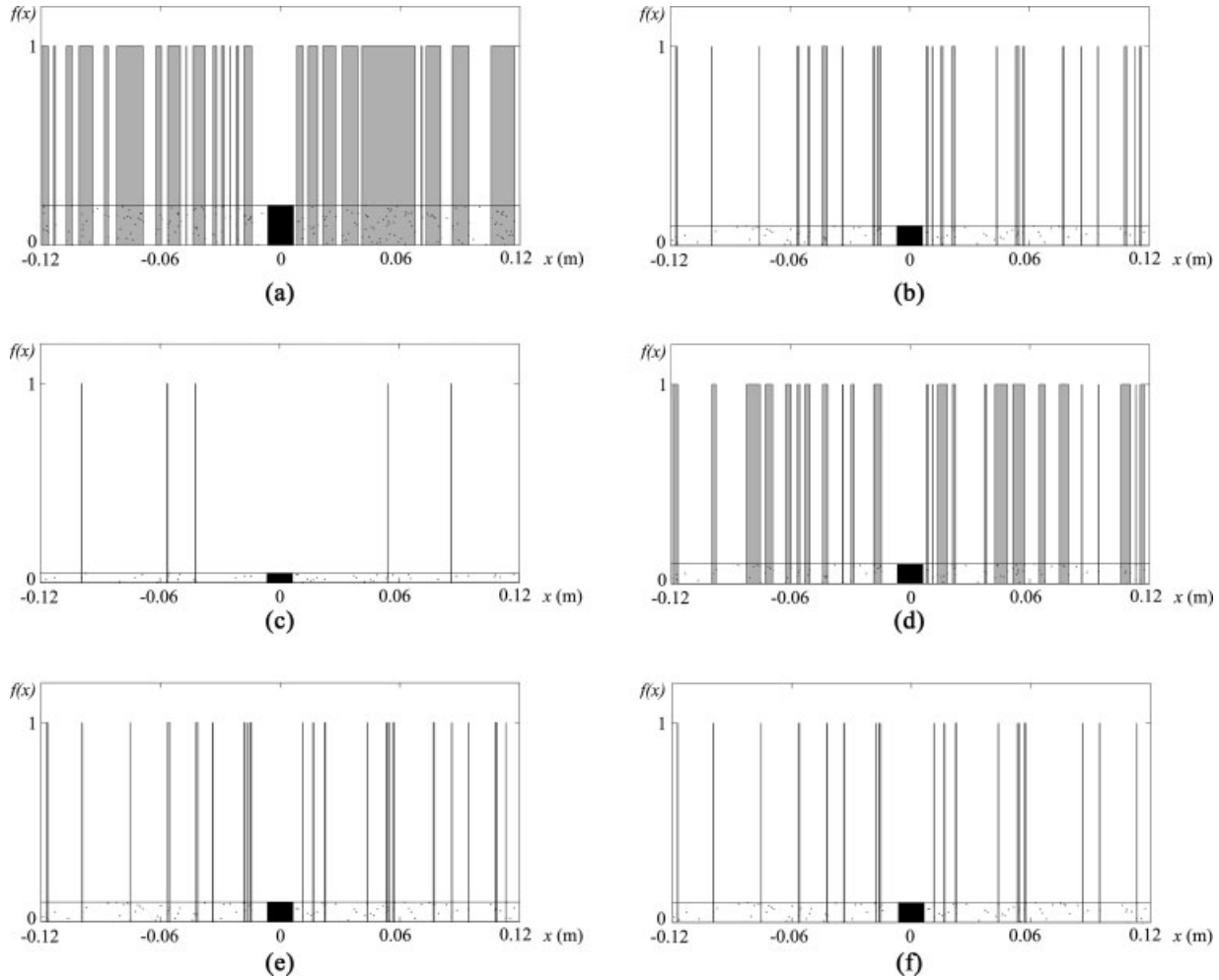


**Figure 10. Striation thickness in the tank at a resolution of (a) $\Delta x = \Delta z = 2$ mm, (b) $\Delta x = \Delta z = 1$ mm, (c) $\Delta x = \Delta z = 0.5$ mm, (d) $\Delta x = 2$ mm, $\Delta z = 1$ mm, (e) $\Delta x = 0.75$ mm, $\Delta z = 1$ mm, and (f) $\Delta x = 0.5$ mm, $\Delta z = 1$ mm.**

The function $f(x)$ is plotted for the transect at $z = 2T/3$ at $Nt = 60$. To compare the striation function $f(x)$ with the real particle distribution in the vessel, the particle positions in the transect are shown at the bottom. The width of the transect is not to scale. The black area at the center of the transect is a part of the shaft.

in Figure 3. The 2 mm resolution, is, therefore, too coarse. A resolution of $\Delta x = \Delta z = 0.5$ mm detects only five very thin striations, as shown in Figure 10c, but since on average a transect that is only half as thick as the mean particle spacing will detect particles only half of the time, this is also a nonphysical result. The resolution of $\Delta x = \Delta z = 1$ mm, shown in Figure 10b, has an exact physical meaning. It corresponds to the mean interparticle distance in the case of a homogeneous distribution, and results in a number of striations with small thicknesses. This $\Delta z$ is used for further calculations.

The effect of $\Delta x$ is illustrated by comparing Figure 10b, d–f. It can be seen that as the resolution in the $x$-direction increases, the striation thicknesses decrease. Weighing the physical meaning of a striation, the $\Delta x$ resolution should be smaller than the mean particle spacing to indicate that two particles are closer together than expected. Comparing the results for $\Delta x = 1$ mm, 0.75 mm, and 0.5 mm (b, e and f) shows very little change in the $f$ profiles. The maximum striation thicknesses give a closer view of the differences between these $\Delta x$'s.

Figure 11 presents the evolution of the maximum striation thickness. The curves with coarser resolution, in either the $z$- or $x$- directions, return higher values of maximum striation thicknesses. With the resolution of $\Delta x = \Delta z = 2$ mm, the maximum striation thickness on the transect decreases at the beginning but starts to increase rapidly as the particles get spread out more evenly. This is nonphysical and indicates that the resolution is too coarse. When $\Delta z$ is reduced to 1 mm, the mean particle spacing, the maximum striation thickness follows a more physical evolution, but for $\Delta z = \Delta x = 0.5$ mm, the striations essentially disappear after $Nt = 10$. A similar evolution is observed when a constant $\Delta z = 1$ mm is used, and the $x$ resolution is varied from $\Delta x = 2$ mm to 1 mm, 0.75 mm and 0.5 mm. For $\Delta x$ less than the mean particle spacing, no significant reduction in the scale of segregation is detected after 10 or 20 impeller revolutions. From a visual examination of the particle distributions in Figure 6 and Figure 3, it is clear that this is not true, but the particle density is quite sparse at the smaller scales of segregation. Comparing the striation thickness curves with the $CoV$ results

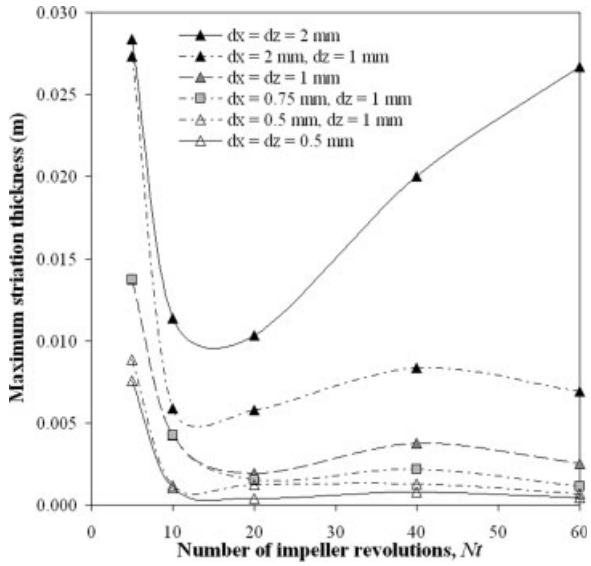


**Figure 11. Maximum striation thickness on the transect located at $z = 2/3H$ for varying transect and striation resolutions (a) $\Delta x = \Delta z = 0.5$ mm, 1 mm and 2 mm, and (b) comparison of the previous plot with curves resulting from a fixed transect width $\Delta z = 1$ mm.**

The mean interparticle distance in the tank is 1 mm.

in Figure 8 reveals that the *CoV* is more sensitive to the later stages of turbulent mixing than the decay of maximum striation thickness on a single transect. The post-processing computational requirement for the accurate calculation of *CoV* is, however; much higher.

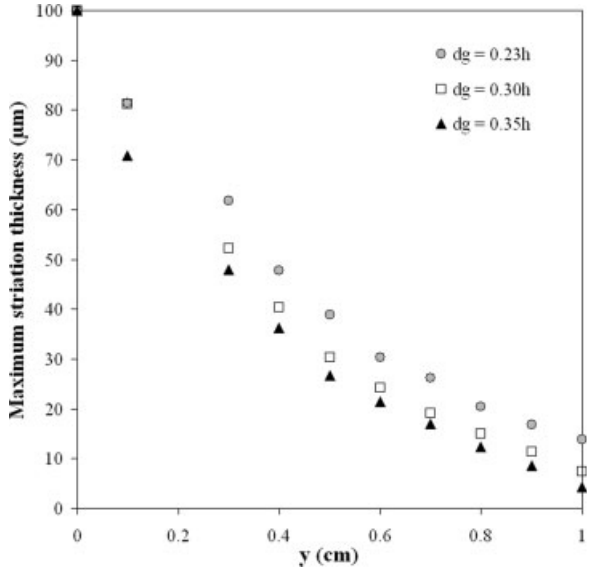


**Figure 12. Maximum striation thickness decay in the micromixer on a transect of width $\Delta z = \Delta x = 5$ $\mu$m for a microchannel of 77 $\mu$m × 200 $\mu$m with 2 480 particle tracks, and an interparticle distance of approximately 2.5 $\mu$m.**

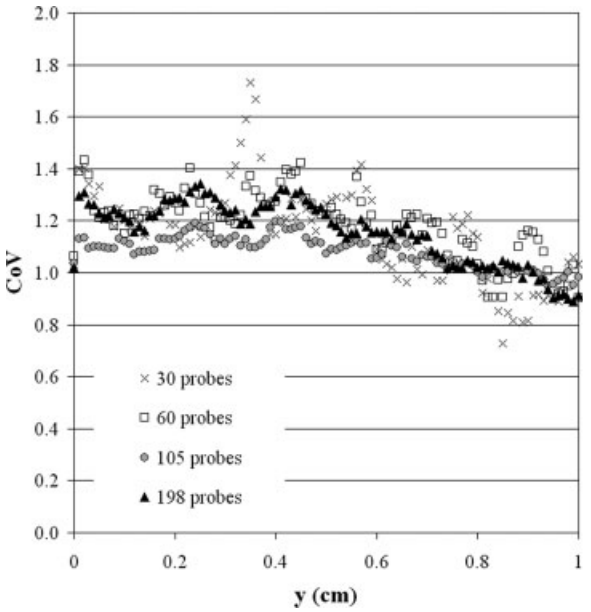


**Figure 13. Influence of the number of probes on *CoV* in the micromixer for a constant 10-particle probe size ($d = 8.89$ $\mu$m), $d_g = 0.23h$.**

The transect results are most meaningful when the width, $\Delta z$, is set equal to the mean particle spacing, and the interparticle spacing threshold is set to be equal to or less than the mean particle spacing. The finest spatial resolution of a transect can be no finer than the mean particle spacing in the flow. The maximum striation thickness within these constraints is not sensitive to the interparticle spacing threshold, and the *CoV* provides more information about the scale

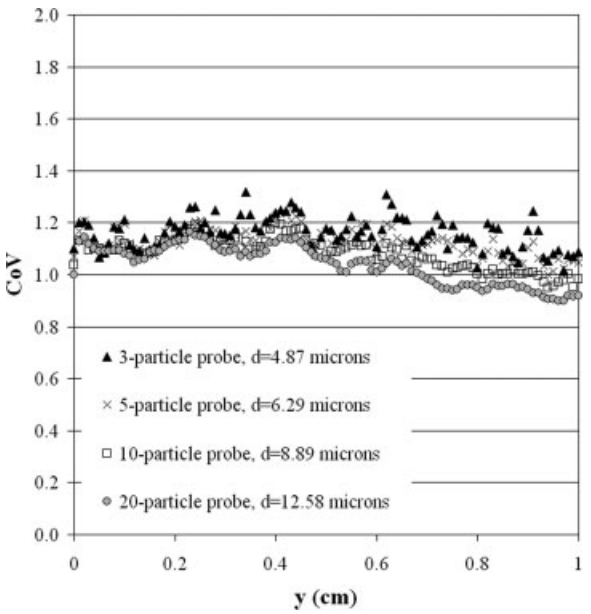


**Figure 14. Influence of the number of particles in the probe on *CoV* for a constant number of 105 probes in the micromixer, $d_g = 0.23h$.**

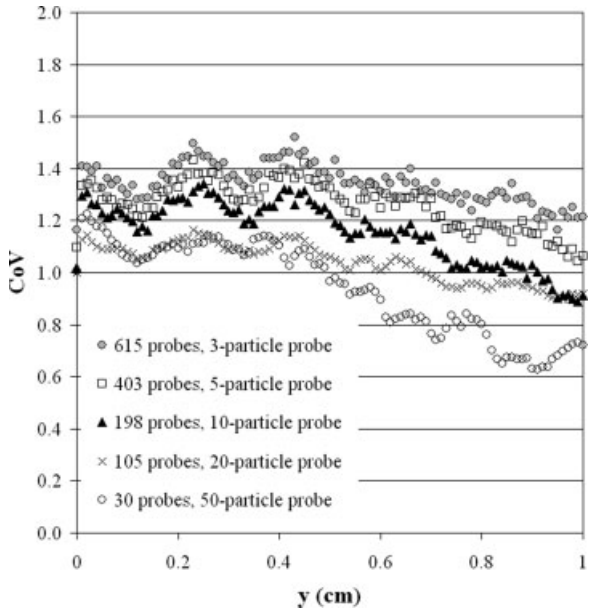


**Figure 15. Effect of the probe size on CoV when the maximum number of probes is used so that the whole population in the micromixer cross-section is sampled; $d_g = 0.23h$.**

reduction stage of mixing than the direct measure of maximum striation thickness on a single transect.

### *Laminar mixing: Transect results*

Figure 12 shows the evolution of the maximum striation thickness along the length of the micromixer. The striation thickness calculation in the micromixer was performed using a single resolution of $\Delta z = \Delta x = 5$ $\mu$m which is twice the mean particle spacing. The larger transect width was needed to capture enough particles to give good resolution of individual striations as observed visually. The maximum striation thickness decreases exponentially as the fluid passes along the mixer. This is characteristic of chaotic flows. This is in contrast with the turbulent case, where the decay in both *CoV* and maximum striation thickness is initially quite sharp, and then levels off. In the laminar micromixer, volume filling and scale reduction happen simultaneously, and the decay in the maximum striation thickness is a much smoother curve.

As the groove depth $d_g$, of the mixer increases, the maximum striation thickness at any position along the mixer decreases. This is in agreement with the qualitative visualizations of the spatial distribution of flow followers made by Aubin.[7] The ability of the different mixer designs to reduce striation thickness and improve mixing performance in the laminar micromixer can be clearly distinguished by tracking the decay of the maximum striation thickness, even at this coarse resolution of twice the mean particle spacing. This result is quite different from the turbulent case.

### *Laminar mixing: CoV results*

The intensity of segregation in the laminar micromixer was determined at different positions using both the quadrat and probe sampling strategies. The spatial positions of the flow followers on 100 equally spaced cross-sections along the mixer were available for each geometry.

Figure 13 shows the influence of the number of 10-particle probes on the *CoV* for the laminar herringbone micromixer. When less than 105 probes are used, the *CoV* curves are

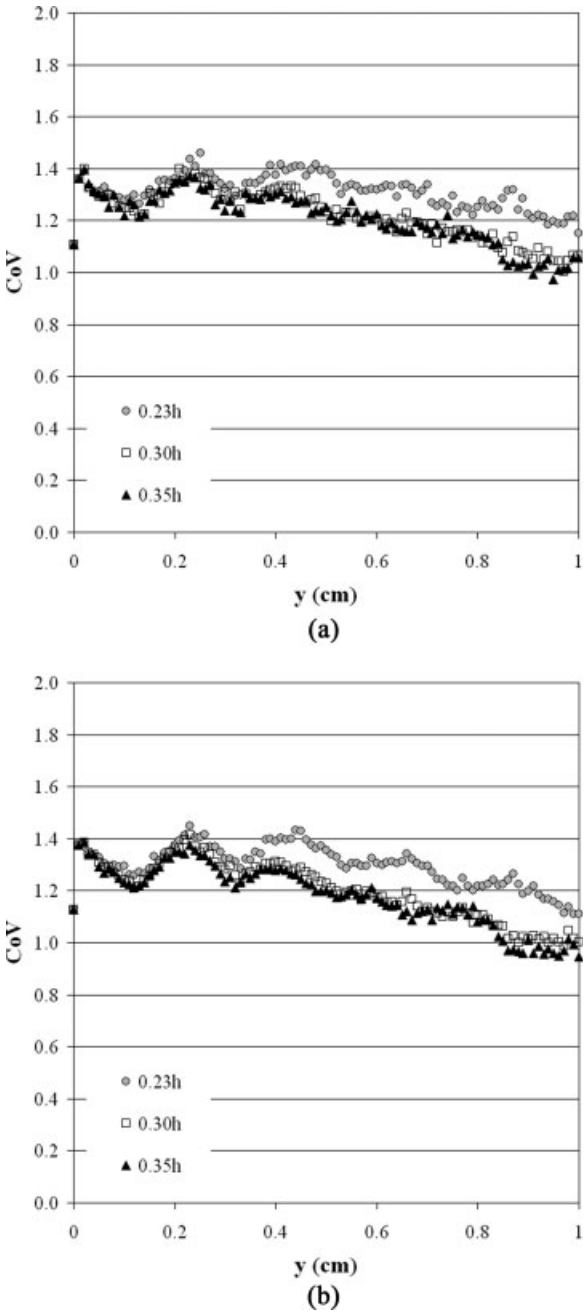


**Figure 16. Comparison of the *CoV* calculated using 640 probes (a) vs. the *CoV* calculated using 640 quadrats (b).**

The probes have a size equivalent to a circle containing 2.92 particles, while the quadrats contain an average of 3.88 particles. The quadrat calculation gives the true population *CoV* at the smallest statistically meaningful scale of measurement for this number of tracer particles.

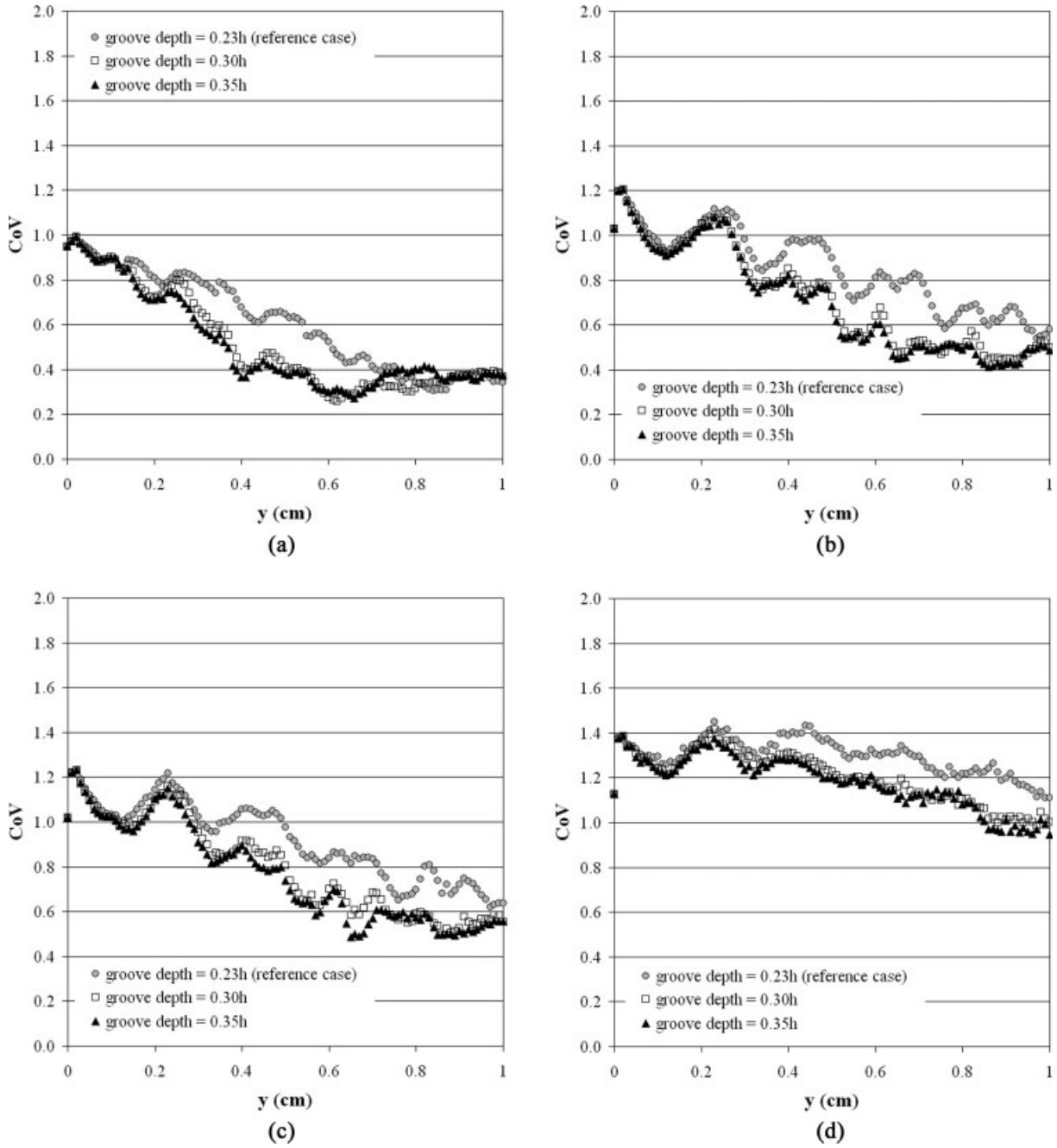


**Figure 17. Influence of the number of quadrats (and quadrat size) on the *CoV* for varying groove depths (a) 10 quadrats with dimensions 40 $\mu$m × 40 $\mu$m, (b) 24 quadrats − 25 $\mu$m × 25 $\mu$m, (c) 40 quadrats − 20 $\mu$m × 20 $\mu$m, and (d) 640 quadrats − 5 $\mu$m × 5 $\mu$m.**

noisy. The curves for 105 and more probes tend to converge after 0.6 cm. Although there is an overall decrease in *CoV* along the mixer, fluctuations of the *CoV* are clearly visible. These fluctuations are periodic and correspond to the periodicity of the staggered herringbone geometry. The magnitude of these fluctuations decreases along the mixer length.

The effect of the probe size on the *CoV* is shown in Figure 14. In this figure, the number of probes is constant and equal to 105. As for the turbulent stirred tank case, the smaller probe size and thus the finer scale of resolution results in a higher *CoV*. For small probe sizes, the *CoV* curves are noisy and are clearly affected by the relative importance of the local concentration fluctuations, as well as statistical error. As the probe size increases, the noise is damped and the curves become smoother. It should be pointed out that a reduction in noise and the consequent smoothing of the *CoV* with increasing probe size was not observed in the previous turbulent flow example, because the *CoV* was determined at only six distinct time steps separated by relatively large time intervals.

The combined effect of the probe size and number is shown in Figure 15. For each probe size, the number of probes was maximized such that almost all of the area in the data plane was sampled. Only the small areas between the non overlapping circles remained unsampled. As the probe size increases, the *CoV* decreases because the concentration fluctuations are averaged over increasingly larger probe areas. In the previous section on turbulent mixing, it was recommended that the probe size be set to the smallest scale of interest, and to have at least 10 particles per probe. Considering the maximum striation thickness in the micromixer geometry at the end of the mixer (Figure 12), the probe size for this case would need to be of the order of 5 $\mu$m. With the current simulations, which used 2,480 flow followers, this probe size would contain less than three particles. In order to obtain higher spatial resolution and reduced statistical error, the number of flow followers used in this simulation would have to be increased.

Because it is not possible to sample the entire data plane with circular probes, the point probe method and the quadrat sampling method are compared in Figure 16. The spatial resolution was fixed to be the smallest possible for the given data set, i.e., 640 probes or quadrats. The mean number of particles expected in one circular probe area is 2.92 and 3.88 particles can be expected in one quadrat. As was mentioned earlier, probes or quadrats with a concentration of three particles are not enough for sampling if a limited number of probes are used. However, in this case the whole population is sampled, and, therefore, the result reflects the true standard deviation of the data even though the probe size is small. Smoother plots were obtained when using the quadrat method than with the probe method because quadrats sample the entire area occupied by the population, which is greater than the total area sampled by the circular probes. As a result, the concentration is averaged over a slightly larger area when using quadrats and the *CoV* is less noisy. Nevertheless, there is little difference in the resulting *CoV* when using either the quadrat sampling or probe sampling, providing that the probe diameter is the largest possible without overlapping of the circular areas. This shows that the shape of the probes/quadrats does not play an important role if a large number of sampling probes/quadrats is used and their size is matched to the smallest scale of mixing.

Figure 17a–d show the effect of quadrat size (and, therefore, spatial resolution) on the *CoV* while comparing the performance of micromixers with different groove depths. Grids of 10, 24, 40 and 640 quadrats have a quadrat size of 40 $\mu$m $\times$ 40 $\mu$m, 25 $\mu$m $\times$ 25 $\mu$m, 20 $\mu$m $\times$ 20 $\mu$m and 5 $\mu$m $\times$ 5 $\mu$m, respectively. When the grid of 10 quadrats is used (Figure 17a), the *CoV* curves of the different geometries converge to the same value at the end of the mixer. As the number of quadrats increases and the quadrat size approaches the smallest scale of striations, two things happen. The *CoV* increases, and it is easier to differentiate the mixing performance obtained with the deeper grooves (0.30$h$ and 0.35$h$) compared with the groove depth of 0.23$h$. This reinforces the fact that special attention should be paid to the physical meaning of the probe size with respect to the desired level of mixing. The quadrat size of 5 $\mu$m $\times$ 5 $\mu$m (640 quadrats) approaches the scale of the largest striation present at the end of the micromixer with $d_g = 0.35h$. The *CoV* curves for the smallest quadrat size (Figure 17d) show a distinctly better performance of the 0.30$h$ and 0.35$h$ groove depths, relative to the mixer with 0.23$h$ groove depth. However, the differences between the *CoV* of the 0.30$h$ and 0.35$h$ groove depth geometries are not as pronounced as those seen in the maximum striation thickness curves.

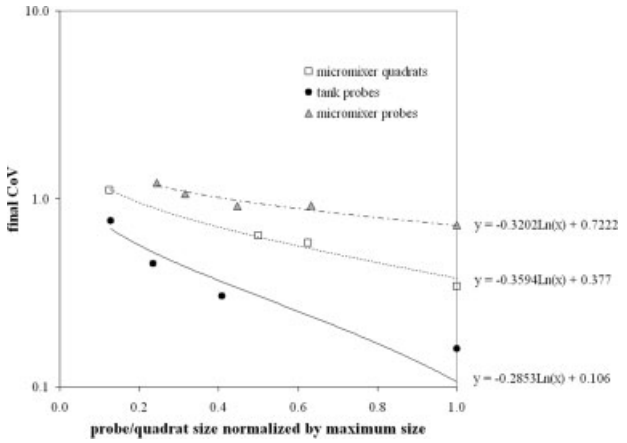


**Figure 18. Effect of probe or quadrat size on the final *CoV* for the stirred tank from Figure 9, and for the laminar micromixer from Figure 15 and Figure 17.**

Figure 18 shows the effect of probe or quadrat size on the final *CoV* value for the stirred tank from Figure 9, and for the laminar micromixers from Figure 15 and Figure 17. In order to show all three curves on one plot, the probe or quadrat size is normalized by the maximum probe/quadrat size used in each case. This normalization changes the $y$-intercept value, but has no effect on the slope of the curves. In all three cases, the final *CoV* decreases logarithmically with an increasing scale of observation.

Figure 18 hints at another important result from the two test cases. The *CoV*, or intensity of segregation, is the dominant characteristic of mixing for the stirred tank, changing by a factor of 5 (from 2.5 to 0.5). In contrast, the *CoV* drops by only 30% over the length of the laminar micromixer (from 1.4 to 1.0). The maximum striation thickness dominates for the laminar micromixer, dropping by a factor of 10 over a smooth progression, whereas for the stirred tank, no change in maximum striation thickness could be detected after the initial volume filling stage ($Nt < 10$). The most useful data is obtained in each case from the measurement which changes the most in the later stages of mixing: intensity of segregation for the turbulent case, and scale of segregation for the laminar case.

## Conclusions

The objectives of this investigation were to explore the data resolution and sampling protocols needed to get accurate measures of *CoV* and striation thickness for two ideal data sets, one turbulent and one laminar; and then to compare the *CoV* and striation thickness results to better understand the strengths and weaknesses of each approach. The results allow us to define accurate sampling methods for a variety of applications in laminar and turbulent mixing.

For the turbulent tank data, the calculated *CoV* depends on the number of probes, the probe size, and the probe placement. The *CoV* based on 3 or 6 probes is far different from the *CoV* obtained from a full field measurement. A small number of probes should only be used to define the perfectly homogeneous endpoint, and accurate determination of the endpoint requires that at least one probe is located in a worst mixed region. The smaller the number of probes used, the tighter the tolerance on the endpoint should be to ensure accurate results. To fully sample the mixing field as it evolves, a minimum of 250 probes were needed for the test data set.

For the laminar micromixer, the *CoV* also depended on the number of probes and the probe size. When the true population *CoV* was measured, it accurately tracked oscillations in *CoV* over each mixing element, and a steady decay over the length of the mixer. Note that the purely logarithmic decay of *CoV* postulated by Eq. 6 is based on data taken at integer numbers of static mixing elements. These data necessarily omits the local oscillations in *CoV*.

For both cases, the *CoV* increases as the probe size shrinks and smaller scales of variation are detected. The absolute value of the final *CoV* changed by up to four times as the probe size was varied. This serves to emphasize the importance of identifying the smallest scale of interest before beginning experiments or simulations. For a laminar mixing field, this scale is the largest acceptable striation thickness. Once this scale is identified, the probe or quadrat size must match the smallest scale of interest. If discrete particle concentrations are being used to determine the *CoV*, the number of particles required for the simulation should be set to allow at least 10 particles to populate each probe area in a perfectly homogeneous distribution. Again, to track the evolution of *CoV*, enough probes must be used to fully sample the mixing field of interest.

Striation thickness measurements provide an alternate measure of mixing, as they focus on the scale of segregation rather than the intensity of segregation. The maximum striation thickness measured depended on both the transect width and the particle separation threshold, $\Delta x$. Based on the results, a transect width, $\Delta z$, equal to the mean particle spacing is recommended, with a particle spacing threshold of $\Delta x \leq$ (mean particle spacing). This means that, on average, a particle will be detected in the 2-D slice, and only particles closer together than expected will be assigned to the same striation. As with the *CoV*, the number of particle tracks required for a simulation can be determined directly if the smallest mixing scales of interest are known.

Two stages of mixing were directly observed in the test data: volume filling, or macromixing, and reduction in scale, or mesomixing. In the turbulent case, the volume filling stage happens quickly, while the scale reduction process is slower. The tank shows an initial rapid decay in *CoV* followed by slower reduction in intensity of segregation. In the static mixer, the self-similarity, or fractal nature of the mixing field means that volume filling and scale reduction happen simultaneously so the two stages cannot easily be distinguished. These observations suggest that "macromixing" be redefined as the volume filling stage of mixing, "mesomixing" as the scale reduction stage, which in turbulent mixing is closely related to the inertial convective range of eddies and in laminar mixing is closely related to the striation thickness distribution, and "micromixing" be defined as the stage of mixing when the scale of segregation is reduced to a point where molecular mechanisms such as viscous dissipation and molecular diffusivity become dominant.

The most useful mixing data was obtained from the measurement which changes the most in the later stages of mixing: intensity of segregation, or *CoV*, for the turbulent case and scale of segregation, or maximum striation thickness on a transect, for the laminar case.

## Acknowledgments

The authors wish to thank Jos Derksen and Hugo Hartmann for providing mixing data.

## Notation

$A$ = entire sampling area available, $m^2$
$A_k$ = area of probe containing $k$ particles, $m^2$
$C$ = concentration, mol/L
$\overline{C}$ = average concentration, mol/L
$C_{imp}$ = impeller off-bottom clearance, m
$C_v$ = volume fraction of unmixed additive
$CoV$ = coefficient of variance
$CoV_r$ = relative reduction in the coefficient of variance
$d$ = probe diameter, m
$d_g$ = microchannel groove depth, $\mu$m
$d_p$ = particle diameter, m
$D$ = impeller diameter or pipe diameter, m
$h$ = microchannel height, $\mu$m
$H$ = tank height, m
$k$ = number of particles in probe
$K$ = constant
$L$ = length, m
$m$ = measurement location number
$M$ = total number of measurement locations
$N$ = impeller rotational speed, rps or rpm
$N_P$ = dimensionless power number
$p$ = total number of particles in area $A$
$t$ = time, s
$T$ = tank diameter, m
$w$ = microchannel width, m
$W_g$ = microchannel groove width, $\mu$m
$x, y, z$ = Cartesian coordinates, m

### *Greek letters*

$\theta$ = tangential position in tank (°)
$\theta_{95}$ = blend time to reach 95% homogeneity, s
$\rho$ = density, $kg/m^3$
$\sigma$ = standard deviation
$\sigma_M^2$ = normalized concentration variance

## Literature Cited

1. Ogawa K. *Chemical Engineering: A New Perspective*. Amsterdam: Elsevier; 2007.
2. Ottino JM. *The Kinematics of Mixing: Stretching, Chaos, and Transport*. Cambridge Texts in Applied Mathematics. Cambridge; New York: Cambridge University Press; 1989.
3. Szalai ES, Alvarez MM, Muzzio FJ. Laminar mixing: A dynamical systems approach. In: Paul EL, Atiemo-Obeng VA, Kresta SM, eds. *Handbook of Industrial Mixing: Science and Practice*. Hoboken, NJ: John Wiley & Sons, Inc; 2004:89.
4. Baldyga J, Bourne JR. *Turbulent Mixing and Chemical Reactions*. New York: John Wiley & Sons, Inc; 1999.
5. Ramkrishna D. *Population balances*. New York: John Wiley & Sons, Inc; 2001.
6. Fox RO. *Computational Models for turbulent reacting flows. Cambridge series in chemical engineering*. Cambridge: Cambridge University Press; 2003.

7. Aubin J, Fletcher DF, Xuereb C. Design of micromixers using CFD modelling. *Chem Eng Sci*. 2005;60:2503–2516.
8. Danckwerts PV. The effect of incomplete mixing on homogeneous reactions. *Chem Eng Sci*. 1958;8:93–102.
9. Arratia PE, Gollub JP. Statistics of stretching fields in experimental fluid flows exhibiting chaotic advection. *J Stat Phys*. 2005;121:805–822.
10. Diggle PJ. *Statistical analysis of spatial point patterns*. New York, NY: Oxford University Press; 2003.
11. Kresta SM, Aubin J. Mixing as a discipline: emerging from the essentials of equipment design to fundamental control of the scale of segregation. 56th Canadian Chemical Engineering Conference: Sherbrooke, Quebec, Canada; 2006.
12. Brown DAR, Jones PN, Middleton JC, Papadopoulos G, Arik EB. Experimental Methods. In: Paul EL, Atiemo-Obeng VA, Kresta SM, eds. *Handbook of Industrial Mixing: Science and Practice*. Hoboken, NJ: John Wiley & Sons, Inc; 2004:172.
13. Etchells AW, Meyer CF. Mixing in Pipelines. In: Paul EL, Atiemo-Obeng VA, Kresta SM, eds. *Handbook of Industrial Mixing: Science and Practice*. Hoboken, NJ: John Wiley & Sons, Inc; 2004:410.
14. Etchells AW, Meyer CF. Mixing in Pipelines. In: Paul EL, Atiemo-Obeng VA, Kresta SM, eds. *Handbook of Industrial Mixing: Science and Practice*. Hoboken, NJ: John Wiley & Sons, Inc; 2004:413.
15. Clements FE. *Research Methods in Ecology*. Lincoln, Nebraska: The University Publishing Company; 1905.
16. Hessel V, Hardt S, Lowe H, Schonfeld F. Laminar mixing in different interdigital micromixers: I. Experimental characterization. *AIChE J*. 2003;49:566–577.
17. Reardon SF, O'Sullivan D. Measures of spatial segregation. *Socio Method*. 2004;34:121–162.
18. Wong DWS. Comparing traditional and spatial segregation measures: A spatial scale perspective. *Urban Geography*. 2004;25:66–82.
19. Mead R. Test for spatial pattern at several scales using data from a grid of contiguous quadrats. *Biometrics*. 1974;30:295–307.
20. McGarvey R, Byth K, Dixon CD, Day RW, Feenstra JE. Field trials and simulations of point-nearest-neighbor distance methods for estimating abalone density. *J Shellfish Res*. 2005;24:393–399.
21. Hilderman TL, Wilson DJ. Simulating concentration fluctuation time series with intermittent zero periods and level dependent derivatives. *Boundary-Layer Meteor*. 1999;91:451–482.
22. Hilderman TL, Hrudey SE, Wilson DJ. A model for effective toxic load from fluctuating gas concentrations. *J Hazardous Mat*. 1999;64:115–134.
23. Hartmann H, Derksen JJ, Van den Akker HEA. Numerical simulation of a dissolution process in a stirred tank reactor. *Chem Eng Sci*. 2006;61:3025–3032.
24. Grenville RK, Nienow AW. Blending of Miscible Liquids. In: Paul EL, Atiemo-Obeng VA, Kresta SM, ed. *Handbook of Industrial Mixing: Science and Practice*. Hoboken, NJ: John Wiley & Sons, Inc; 2004:509.
25. Kresta SM, Mao DM, Roussinova V. Batch blend time in square stirred tanks. *Chem Eng Sci*. 2006;61:2823–2825.
26. Nienow AW. On impeller circulation and mixing effectiveness in the turbulent flow regime. *Chem Eng Sci*. 1997;52:2557–2565.

*Manuscript received Jan. 17, 2008, and revision received July 18, 2008.*